Search for a liquid-liquid critical point in models of silica

Erik Lascaris,[1] Mahin Hemmati,[2] Sergey V. Buldyrev,[3] H. Eugene Stanley,[1] and C. Austen Angell[2]
[1]*Center for Polymer Studies and Department of Physics, Boston University, Boston, Massachusetts 02215, USA*
[2]*Department of Chemistry and Biochemistry, Arizona State University, Tempe, Arizona 85287, USA*
[3]*Department of Physics, Yeshiva University, 500 West 185th Street, New York, New York 10033, USA*

(Received 12 February 2014; accepted 8 May 2014; published online 10 June 2014)

Previous research has indicated the possible existence of a liquid-liquid critical point (LLCP) in models of silica at high pressure. To clarify this interesting question we run extended molecular dynamics simulations of two different silica models (WAC and BKS) and perform a detailed analysis of the liquid at temperatures much lower than those previously simulated. We find no LLCP in either model within the accessible temperature range, although it is closely approached in the case of the WAC potential near 4000 K and 5 GPa. Comparing our results with those obtained for other tetrahedral liquids, and relating the average Si–O–Si bond angle and liquid density at the model glass temperature to those of the ice-like β-cristobalite structure, we conclude that the absence of a critical point can be attributed to insufficient "stiffness" in the bond angle. We hypothesize that a modification of the potential to mildly favor larger average bond angles will generate a LLCP in a temperature range that is accessible to simulation. The tendency to crystallize in these models is extremely weak in the pressure range studied, although this tendency will undoubtedly increase with increasing stiffness. © *2014 AIP Publishing LLC*. [http://dx.doi.org/10.1063/1.4879057]

I. INTRODUCTION

Silica (SiO_2) is one of the most important and widely used materials in today's world. Because silica is an excellent insulator and can be easily created through thermal oxidation of the silicon substrate, SiO_2 is also the insulator of choice in the semiconductor industry. Optical fibers made from pure silica are widely used by the telecommunications industry and, because silica and silicates make up over 90% of the Earth's crust, SiO_2 plays a major role in the geosciences.

Liquid silica is the extreme case of a "strong" liquid. When cooled, its viscosity approaches the glass transition slowly, following the Arrhenius law $\log \eta \propto 1/T$. In contrast, the so-called "fragile" liquids reach this glass transition far more quickly. Glasses rich in silica, but modified by other oxides to lower their viscosities, are "strong" liquids that have slow vitrification so are preferred by glassblowers and glass artists who need time to work their magic.

Simulations have indicated that liquid silica does not behave like a strong liquid for all temperatures, however. Using the BKS model[1] (see Appendix A), Vollmayr *et al.* found that at very high temperatures the diffusion greatly deviates from the Arrhenius law (and thus behaves like a fragile liquid), and that the temperature-dependence of the diffusion better fits the Vogel-Fulcher law.[2] It was later shown by Horbach and Kob[3] that the temperature-dependence can also be fitted well by a power law of the shape $D \propto (T - T_{\mathrm{MCT}})^{\gamma}$ in which the exponent γ is close to 2.1 (compared to 1.4 for water) and $T_{\mathrm{MCT}} \approx 3330$ K. This temperature dependence is often found in simple liquids and has been described in terms of mode-coupling theory (MCT).[4,5] A deviation from the Arrhenius law has also been measured in other models of silica,[6] and small deviations from a pure Arrhenius law were found for the viscosity in experimental data.[7,8] This transition from fragile to strong upon cooling (often called the "fragile-to-strong crossover") has also been found in simulations of other tetrahedral liquids, such as BeF_2,[9] silicon,[10,11] and water.[12–14] This phenomenon is not restricted to tetrahedral liquids, however. For example, it has been proposed that the fragile-to-strong crossover might be a behavior common to all metallic glass-forming liquids.[15,16]

In addition to the fragile-to-strong crossover, it has been proposed that liquid silica also has a liquid-liquid critical point (LLCP)[17–19] much like that proposed for liquid water.[20] These phenomena may be related. It was recently shown that in analog plastic crystal systems many strong glass-formers are accompanied by a singularity (a lambda-type order-disorder transition) at high temperatures, and that in silica this singularity could be a LLCP.[19] The fragile-to-strong crossover arises simultaneously with a large increase of the isobaric heat capacity C_P. If a LLCP exists in silica, this heat capacity maximum should have its origin in its critical fluctuations. The discovery of a LLCP in liquid silica would thus provide a unifying thermodynamic explanation for the behavior of liquid silica.

II. METHODS

We consider here two different models of silica, the BKS model by van Beest *et al.*[1] and the WAC model (also known as the Transferable Ion Model (TRIM) model for silica) introduced by Woodcock *et al.*[21] Both models represent SiO_2 as a simple 1:2 mixture of Si ions and O ions, i.e., without any explicit bonds. One difference between the two models is that WAC uses full formal charges, while in BKS partial

charges are used. For a detailed description of both models, see Appendix A.

All simulations are done using Gromacs 4.6.1,[22] with $N = 1500$ ions, using the Ewald sum (PME) for electrostatics, and the v-rescale thermostat[23] to keep the temperature constant. Most simulations are done in the constant-volume/constant-temperature (NVT) ensemble. For the few constant-pressure (NPT) simulations we use the Parrinello-Rahman barostat. For most of the simulations we use a time step of 1 fs, but at very low temperatures we increase the time step to 4 fs to speed up the simulations to approximately 250 ns/day. We carefully check the temperatures below which the 4 fs time step gives the same results as the 1 fs time step and do not include any 4 fs data that lead to a small difference in pressure, energy, or diffusion.

As a measure of the equilibration time, we define τ as the time at which $\sqrt{\langle r_O(t)^2\rangle} = 0.56$ nm, i.e., the average time it requires for an O ion to move twice its diameter of 0.28 nm. Most simulations run for over $10\,\tau$, well beyond the time necessary for the system to reach equilibrium. For the range of temperatures and pressures considered here, the root mean squared displacement of the O ion is roughly 1.1–1.6 times that of the Si ion, this factor being the largest at low temperatures and low pressures.

An important structural feature is the coordination number of Si by O, since a tetrahedral network is defined by 4-coordination of the network centers. We calculate the Si coordination number by the usual method, integrating the Si–O radial distribution function up to the first minimum. For both models, and at all state points considered here (below 10 GPa), the coordination number lies between 4.0 and 4.9. The coordination number is largest at high densities, and levels off to 4 when the density is decreased and the pressure reaches zero and becomes negative.

III. ISOCHORES

The most direct method of locating a critical point is to calculate the pressure P as a function of temperature T along different isochores. In a PT-diagram the isochores cross within the coexistence region and at the critical point.[53,54] At those state points (at a given P and T), the system is a combination of two different phases with different densities. One can also locate a critical point by plotting the isotherms in a PV-diagram in order to determine the region in which the slope of the isotherms becomes zero (critical point) or negative (coexistence region). Because it is easier to determine whether two lines are crossing than whether a curve is flat, we study the isochores. Figure 1 shows the PT-diagrams with the isochores of BKS and WAC.

Both diagrams are similar. There is a clear density anomaly to the left of the temperature of maximum density (TMD), and if we shift the temperature scale for BKS by approximately +4000 K, then the BKS isochores match those of WAC reasonably well. At very low P and high T, the liquid phase is bounded by the liquid-gas (or liquid-vacuum) spinodal, and lowering P below the spinodal leads to spontaneous bubble formation. At very low T the diffusion coefficient drops rapidly and the liquid becomes a glass. Because

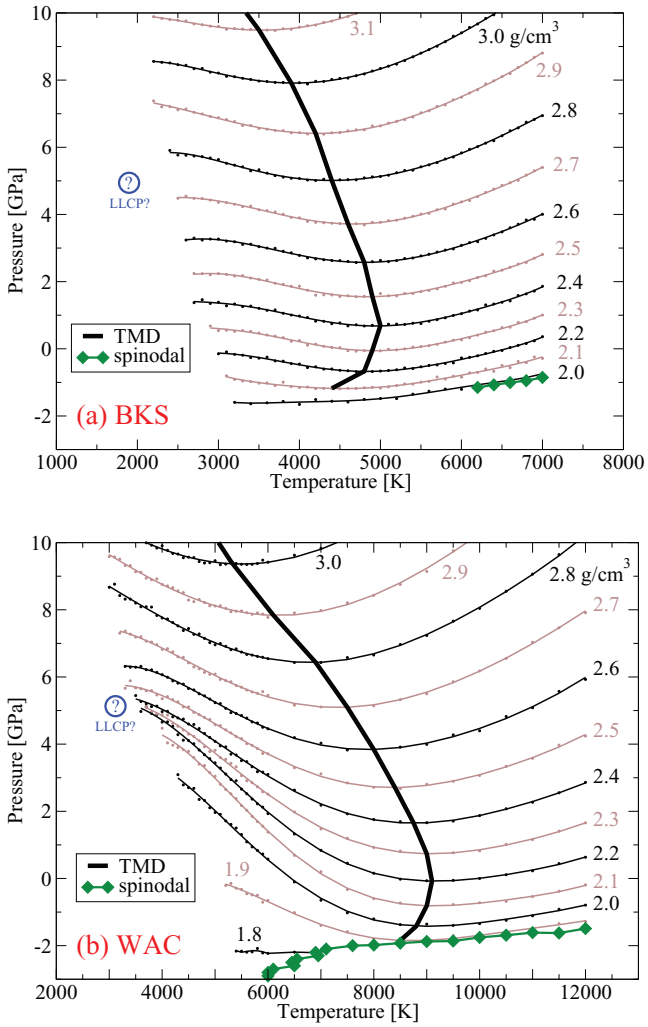

FIG. 1. Isochores of liquid BKS silica (panel a) and liquid WAC silica (panel b). Thin black/brown lines are the isochores, the temperature of maximum density (TMD) is indicated by a thick black line, and green diamonds indicate part of the liquid-vacuum spinodal. Blue question marks indicate the approximate locations where a LLCP has been predicted by previous studies.[18,19] The location of a LLCP can be identified by where the isochores cross. It seems a LLCP in BKS is unlikely, as the isochores do not approach each other. The isochores in WAC do approach each other, and might converge at the predicted point. However, at low temperatures the isochores near 2.3 g/cm^3 obtain a negative curvature. If this curvature becomes more negative as T goes down, then it is possible that the isochores will not cross below 3500 K. We conclude that for the temperatures currently accessible, the isochores alone are insufficient to demonstrate a LLCP in WAC.

the time it takes to equilibrate the system is inversely proportional to the rate of diffusion, simulations require too much time once the oxygen diffusion D_O drops below $\sim 10^{-8}$ cm^2/s, which is where the isochores stop in Fig. 1. For both models this limit is reached at a higher temperature for low P than for high P. This is caused by the diffusion anomaly (an increase in P leads to an *increase* in diffusion), which is present in both BKS and WAC models.

No crystallization was observed, unless the pressure was raised to values far outside the range of our detailed studies (e.g., above 40 GPa the WAC liquid spontaneously crystallizes into an 8-coordinated crystal). Normally, crystallization is readily detected by a rapid drift of the energy to lower values. However, when the diffusivity is very low (as in the

present system, in the domain of greatest interest), the situation is different and crystal growth can be unobservably slow. More direct tests are then needed. In the present case, we have sought information on crystal growth and melting by creating a crystal front (half simulation box of the liquid interfacing with half box of the topologically closest crystal) and have watched the crystal front receding at high temperature. However, the attempt to determine melting point by lowering the temperature and observing reversal of the interface motion was unsuccessful because the growth rate became unobservably small (observed over microseconds) before any reversal was seen. We conclude that, since this crystal front was put in by hand, the possibility of crystallization by *spontaneous* nucleation (always the slowest step) followed by crystal growth, is zero.

Based on the fitting and extrapolation of data, previous studies have predicted a LLCP in both WAC and BKS.[18] With the increase in computing power, and using the techniques to speed up the simulations discussed in Sec. II, we are able to obtain data at lower temperatures than was previously possible. Our results for BKS (Fig. 1(a)) show that for $T > 2500$ K the isochores are nearly parallel, and therefore a LLCP in BKS is very unlikely. On the other hand, the isochores of the WAC model (Fig. 1(b)) show a more interesting behavior in that they clearly approach one another at low T in the vicinity of $P \approx 5$ GPa.

If we only consider the WAC isochores above 4000 K, then extrapolation would predict that the isochores cross around 3500 K and 5 GPa. However, below 4000 K we see that the isochores are starting to display a negative curvature in the PT-plane. This signals an approach to a density minimum, which is the low-T boundary of the density anomaly region. The negative curvature makes it hard to perform an extrapolation that convincingly shows that the isochores cross at lower T. We can therefore only conclude that (for the temperatures currently accessible), the behavior of the isochores is insufficient to prove or disprove the existence of a LLCP in WAC.

IV. RESPONSE FUNCTIONS

Upon approaching a critical point, the response functions diverge. Although true divergence occurs only in the thermodynamic limit $N \to \infty$, a large maximum should still be visible in response functions such as the isothermal compressibility K_T and the isobaric heat capacity C_P even when the box size is relatively small. Calculations using the Ising model and finite size scaling techniques applied to simulation results have shown that (for sufficiently large boxes) the location of the critical point is very close to where both K_T and C_P reach their global maximum.[55,24,25] If a LLCP truly exists for the WAC model, then the PT-diagrams of C_P and K_T should show a large C_P maximum close to where K_T has a maximum—exactly where the isochores come together and where the LLCP has been predicted to be.

Figure 2 shows four response functions for WAC: (a) the isothermal compressibility K_T, (b) the isobaric heat capacity C_P, (c) the isobaric thermal expansivity α_P, and (d) the isochoric heat capacity C_V. These have been obtained using NVT simulations together with the smooth surface technique described in Appendix B. To check the results generated by this technique, we determine whether the response functions satisfy the thermodynamic relation $VT\alpha_P^2/K_T + C_V - C_P = 0$. Because of statistical errors in the data we find slight deviations from zero, but these are less than 1 J/(mol K) in magnitude.

The compressibility K_T in Fig. 2(a) shows a clear global maximum near $P \approx 5$ GPa and $T \approx 4000$ K, because this is where the isochores in Fig. 1(b) are the closest together in terms of pressure. It is quite likely that below 4000 K this maximum increases further. If WAC has a LLCP, then C_P should also have a maximum in that vicinity. However, Fig. 2(b) shows that this is not the case. There is clear global C_P maximum, but it is located near $P \approx 1$ GPa and $T \approx 6000$ K, which is far from the global K_T maximum. Therefore, based on the response functions, we conclude that WAC does not have a LLCP.

The isobaric thermal expansivity α_P (Fig. 2(c)) has a global minimum between the global maxima of C_P and K_T (Figs. 2(a) and 2(b)). This should come as no surprise, since $C_P \propto \langle(\Delta S)^2\rangle$ arises from fluctuations in entropy and $K_T \propto \langle(\Delta V)^2\rangle$ from volume fluctuations, while the expansivity $\alpha_P \propto \langle \Delta S \Delta V\rangle$ arises from a combination of both. Even though the global maxima occur at different places, the slopes dP/dT of the loci of local maxima are the same, so it seems likely they have a common origin. Because the system is not quite critical, the enthalpy fluctuations that determine the heat capacity can be statistically independent of the density fluctuations.

The variation of the heat capacity with temperature at constant pressure is shown over the temperature range in which the system remains in equilibrium, in Fig. 3. Fig. 3(b) is basically a cross-section of Fig. 2(b). We note first that at moderately high pressures, 8 GPa, there is no difference between the WAC and BKS models. In each case the heat capacity reaches about 35 J/(K mol) before the diffusion becomes too slow that we can no longer equilibrate. This is 1.4 times the vibrational heat capacity of $3R \approx 25$ J/(K mol), as is typical of moderately fragile inorganic liquids (e.g., anorthite, $ZnCl_2$) right before ergodicity is broken.[26,27] However, at pressures between zero and 5 GPa, a major difference is seen between the models.

Near the TMD we have $C_P \approx C_V$ (because the expansivity is very small) so we can compare data with C_V from Scheidler *et al.*[28] for the case of BKS at $P = 0$. The agreement is quantitative, up to the point where the earlier study was cut off. Our data confirm the existence of a peak in the equilibrium heat capacity—an unusual behavior that was not reported in Ref. 28 but had been noted in the earlier study of Saika-Voivod *et al.*[29] and was emphasized in Ref. 19.

Although BKS is far from having a critical point, the existence of this C_V maximum reveals the tendency of this system—which accords well with many aspects of experimental silica—to develop the same anomalous entropy fluctuations, and an analog of the Widom line made famous by water models.

For the WAC model (which approaches criticality much more closely than BKS does, as we have already seen in

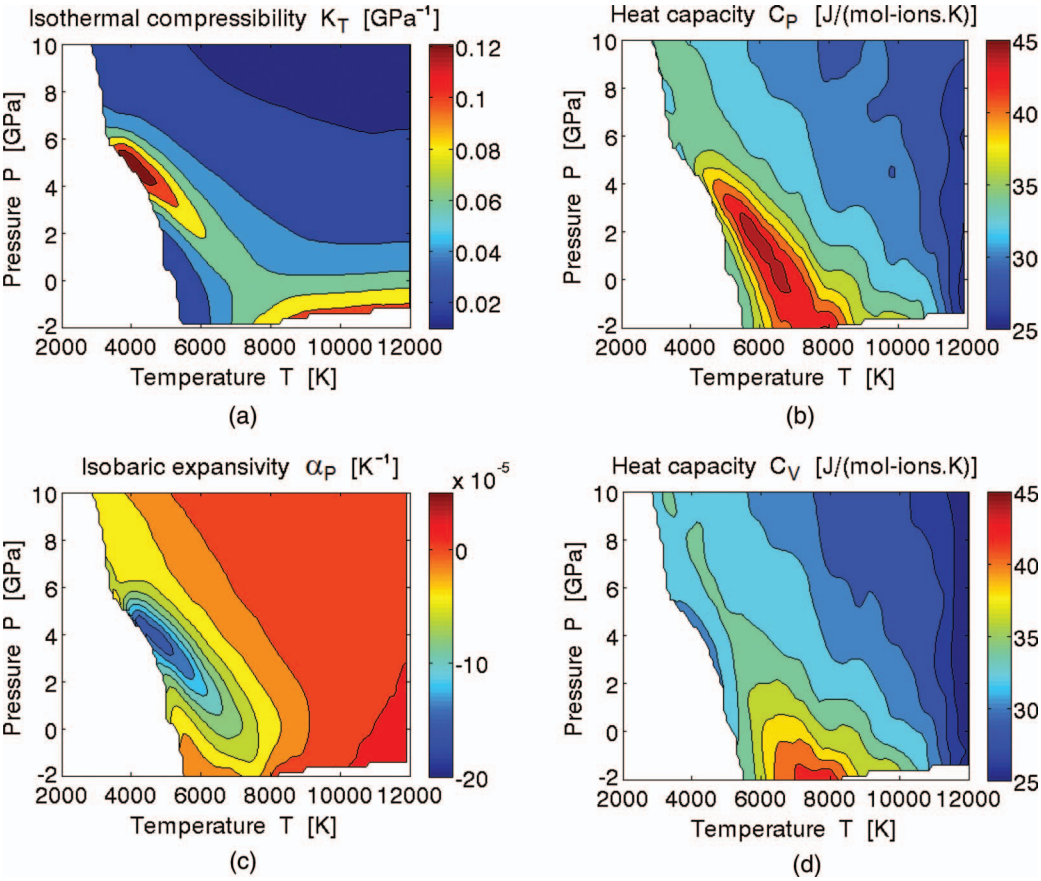

FIG. 2. Response functions of WAC. (a) The isothermal compressibility K_T is consistent with a LLCP near 5 GPa, 4000 K because near that point K_T has a global maximum. (b) The isobaric heat capacity C_P, however, has a global maximum around 1 GPa and 6000 K, far away from where K_T has its global maximum. This is inconsistent with the LLCP hypothesis. (c) The isobaric thermal expansivity α_P has its global minimum in between the global maxima of K_T and C_P. The contour line where $\alpha_P = 0$ corresponds to the location of the TMD. (d) The isochoric heat capacity C_V has its global maximum the furthest away from the global K_T maximum.

Fig. 1), this heat capacity peak becomes much more prominent, reminiscent of the behavior of the Jagla model near its critical point.[56] C_P reaches a value almost twice that of the vibrational component; behavior unseen in any previous inorganic system except for BeF_2 which is a WAC silica analog.[27]

V. DISCUSSION

We find no LLCP in either model within the accessible temperature range, although it is closely approached in the case of the WAC potential near 4000 K and 5 GPa. The isochores of BKS, which are the most direct indicators of criticality in a physical system, fail to converge into a critical point. In the case of WAC, we cannot conclude anything from the isochores, but an analysis of the global extrema of the response functions indicates that there is no LLCP in WAC because the global C_P maximum and the global K_T maximum are significantly separated in the *PT*-plane.

Liquid silica forms a tetrahedral network of bonds, and below we will show that the lack of a LLCP is related to the openness of this network structure, which in turn is related to the stiffness of the inter-tetrahedral bond angles. In addition, we will argue that criticality in WAC could be achieved with an adaptation of the pair potential.

The occurrence of a LLCP requires two competing liquid structures that can be in a (meta-stable) equilibrium with each other. In the case of a tetrahedral network-forming liquid the two relevant structures are usually: (i) a high-density collapsed structure that is highly diffusive and (ii) a low-density open network structure that is more rigid, i.e., one that is still a liquid but less diffusive and more structured. Because the high-density structure occupies a smaller volume but has higher entropy (more disorder), the competition between these two structures is accompanied by a region with a density anomaly: $\alpha_P \propto \langle \Delta S \Delta V \rangle < 0$.

The high-density structure is very stable and is the dominant structure at high temperatures, but the low-density structure requires a more delicate balance of forces in order to be stable. If the bonds in the liquid are too flexible, the liquid collapses into the high-density structure. On the other hand, if the bonds are too rigid the liquid can no longer flow and becomes a glass.

There are several studies that address this situation. The 2006 study of Molinero *et al.*[30] shows how reducing the three-body repulsion parameter λ in the Stillinger-Weber potential[31] (which controls the bond angle stiffness) causes the first order liquid-liquid phase transition of silicon ($\lambda = 21$) to disappear at $P = 0$ when $\lambda < 20.25$ (see Fig. 4). This transition occurs between a low-density liquid and a high-density liquid,

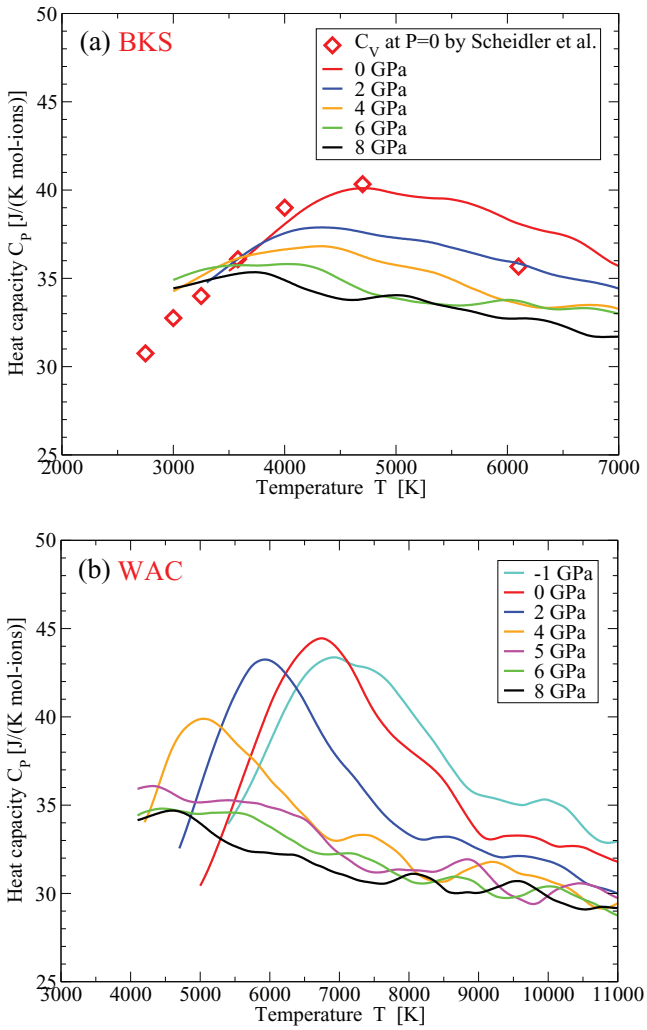

FIG. 3. Comparison of the heat capacities of BKS (panel (a)) and WAC (panel (b)), obtained by calculating the smoothing spline of $H(T)$ at constant P, followed by taking its derivative (a slightly different method than was used in Fig. 2(b)). At 8 GPa, there is no significant difference between the WAC and BKS models, but below 5 GPa WAC has a large maximum in the range 5000–8000 K (also clearly visible in Fig. 2(b)). In panel (b) we have included C_V data of Scheidler *et al.*[28] (red diamonds), which shows a maximum around 4500 K. Near the TMD (around 5000 K for $P = 0$) the expansivity is small, which means that $C_V \approx C_P$, in agreement with our results. For BKS this maximum is less clear in C_P, though still visible. Because of small fluctuations in the data, it is difficult to obtain a fit of $H(T)$ that produces a perfect estimate of $C_P = dH/dT$, leading to artificial oscillations in C_P. A larger data set would reduce this artifact. In addition, the smoothing spline method assumes zero curvature at the end-points of the data, and this leads to artifacts at very low T and very high T. For clarity, we have removed the parts of the curves below the temperature at which C_P starts to bend toward a constant C_P value.

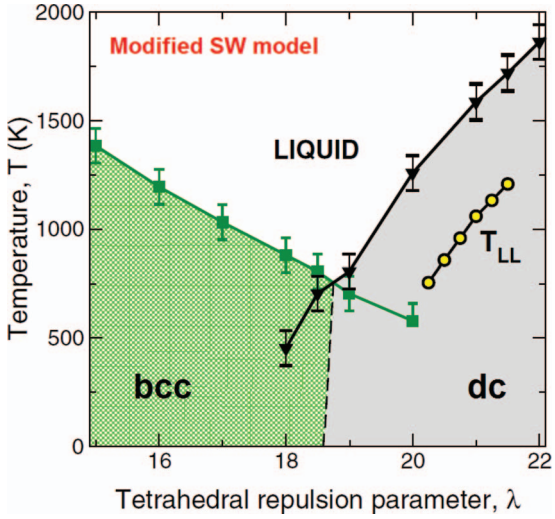

FIG. 4. Phase diagram of the modified Stillinger-Weber potential in terms of the tetrahedral repulsion parameter λ and temperature T, at zero pressure.[30] The black triangles indicate the melting line of the diamond cubic (dc) crystal, while the green squares denote the melting line of the bcc crystal. The dashed line separates the dc and bcc regions. Yellow circles indicate the transition temperature T_{LL} at which the liquid-liquid phase transition line crosses the $P = 0$ isobar for that particular value of λ. Silicon is represented by $\lambda = 21$ and has a liquid-liquid critical point at −0.60 GPa,[32] and therefore all LLCPs for $\lambda > 20.25$ lie at negative pressures (there is a LLCP for each value of λ). For $\lambda < 20.25$ the LLCPs are at positive pressures and therefore the phase transition line can no longer be seen in this diagram. When λ is large the system easily crystallizes, and therefore the phase transition line at $P = 0$ can no longer be accurately located when $\lambda > 21.5$.

where both liquids are metastable with respect to the diamond cubic (dc) crystal. Crystallization to the dc crystal always occurs from the low-density liquid. When $\lambda > 21.5$ crystallization happens so fast that it is no longer possible to accurately determine the temperature T_{LL} at which the phase transition occurs for $P = 0$.

Simulations of the Stillinger-Weber model indicate that the LLCP for $\lambda = 21$ is located at −0.60 GPa and 1120 K.[32] Since each value of λ defines a unique system with a unique critical pressure, the vanishing of the liquid-liquid transition at $\lambda < 20.25$ implies that this is the λ value for which the LLCP is at $P = 0$. Isochore-crossing studies conducted elsewhere[33] show that this is indeed the case, with $T_c \approx 700$ K for $P_c = 0$. It is clear that decreasing λ means decreasing the tetrahedrality and increasing density. When $\lambda < 20.25$ the LLCP shifts to positive pressures, and therefore the phase transition line can no longer be seen in Fig. 4, as it only considers $P = 0$. We thus lack the information to determine exactly for which λ there is no LLCP at *any* pressure, but it is certain that this happens at some value $\lambda > 0$, since in the most extreme case of $\lambda = 0$ we are left with a simple Lennard-Jones-like model that has no LLCP.

That weakening the tetrahedrality (i.e., making the tetrahedral bonds more flexible) leads to the removal of a LLCP, was also shown in 2012 by Tu and co-authors using a different monatomic model.[34] The Hamiltonian of this model includes a term that lowers the energy when particles are aligned along near-tetrahedral angles and thus favors a diamond cubic ground state. The study of Ref. 34 considers two versions: one that allows broad flexibility of the inter-tetrahedral bond angles (leading to weak tetrahedrality), and another in which the bond angle is more constrained (giving rise to strong tetrahedrality).

The behavior for strong tetrahedrality is shown in Fig. 5, and we see that the isochores converge into a critical point. If the tetrahedrality is weakened slightly, then the isochores separate, the LLCP disappears, and the diagram starts to resemble that of Fig. 1(b) for WAC. It should be mentioned that a separation of the global C_P and K_T maxima also occurs in

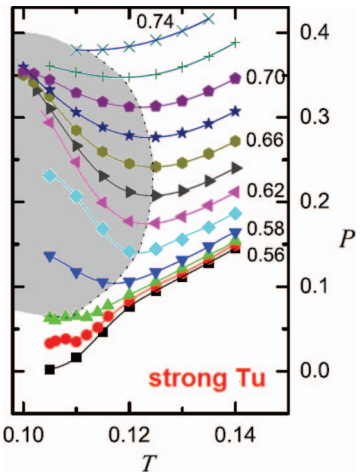

FIG. 5. Isochores of the Tu model for the strong tetrahedrality version, which has a LLCP.[34] Gray area indicates the density anomaly region. By reducing the tetrahedrality, the Tu model can be smoothly changed into the weak tetrahedrality version, which does not have a LLCP. The isochores of WAC (Fig. 1(b)) show no LLCP but closely resembles that of the strong Tu model. We can interpret this as that WAC is *close* to having a LLCP, but not close enough. If we were to enhance the tetrahedrality of WAC, it is likely a LLCP would appear.

the weak tetrahedrality version (as is the case for WAC), while the C_P and K_T maxima are close together and near the LLCP in the strong version of the model.

Finally, we should consider the simulations done on "patchy" colloids by Sciortino and co-workers. Using the Kern-Frenkel (KF) model[35] (which consists of particles with tetrahedrally arranged sticky points), these authors demonstrated that the colloids developed tetrahedral network topologies, with each particle being surrounded by four others—which is not itself surprising. More interesting was the finding that, when the effective sizes of the patches were varied, conditions could be found in which not only were the relaxation kinetics strictly Arrhenius in form, but also the amorphous state became the free energy ground state of the system, over a wide range of densities.[36] This corresponds to a more dramatic stabilization of the amorphous state than the kinetic stability observed in our work. It signifies an absolute stability against crystallization on any time scale, i.e., the system has become an "ideal glassformer."[37]

Studies with the KF model have also demonstrated that highly directional bonds are needed to observe spontaneous crystallization in tetrahedral interacting particles,[38] in agreement with the results found by Molinero *et al.* using the Stillinger-Weber family of potentials. Since the KF colloids can be used to describe different tetrahedral models, they promote our understanding of tetrahedral liquids, such as ST2 and mW water, Stilling-Weber silicon, and BKS silica. Surprisingly, there exists a mapping from these models to the KF model, using only a single parameter: the patch width.[39] The patch width is related to the flexibility of the bonds between the particles, and it is therefore likely that spontaneous crystallization and the existence of a LLCP are related to bond angle flexibility.

All of these studies show that the occurrence of a LLCP becomes less likely when the parameters controlling tetrahedrality are weakened. Unfortunately, the BKS and WAC models do not have an explicit parameter that controls tetrahedrality, such as the parameter λ in the Stillinger-Weber model. In this model, there is a direct relation between the value of λ and the tetrahedrality of the liquid measured by the orientational order parameter q as defined by Errington and Debenedetti.[40] This parameter is constructed such that its average value $\langle q \rangle$ will equal zero if all atoms are randomly distributed within the liquid, while $q = 1$ for each atom within a perfect tetrahedral network (such as in a cubic diamond lattice). For silica the situation is more complicated. It is not immediately clear how to define the tetrahedrality of a system that consists of two types of atoms. One way would be to find for each Si atom its four nearest neighboring Si atoms and compute $\langle q \rangle$ for this subset of atoms. However, this measure would completely ignore the positions of the O atoms which form ionic bridges between the Si atoms. Since the O–Si–O bond angle deviates very little from the perfect tetrahedral angle of 109°,[2] it makes sense to focus on the inter-tetrahedral Si–O–Si bond angle instead. It is commonly agreed that structures such as diamond cubic have maximum tetrahedrality, and for silica this corresponds to a system where all Si–O–Si bond angles are equal to 180° (such as β-cristobalite). How much the inter-tetrahedral Si–O–Si bond angles differ from 180° can thus be employed as a measure of the tetrahedrality, and we have therefore calculated this bond angle distribution for both BKS and WAC. The location of the maximum in the Si–O–Si bond angle distribution (i.e., the most probable angle) is a parameter that one could use to quantify the tetrahedrality. If we denote the most probable angle at the lowest accessible temperature (T_g) as $\theta_{\max}$, then the tetrahedrality parameter t can be defined as $t \equiv \theta_{\max}/180°$, where $0 < t < 1$. Since the "openness" of the structure will increase with the average Si–O–Si angle, one could also define the tetrahedrality using the volume ratio, i.e., $t \equiv V^*/V_{\rm dc}$, which would require much less effort to calculate. Here $V_{\rm dc}$ is the volume of the perfect diamond cubic and V^* is the system volume at some corresponding state, for instance at the TMD (which is less arbitrary than T_g).

Let us consider the angular relations and the mechanical forces that determine them in more detail. In terms of the familiar ball-and-stick model, the Si–O–Si bond could be represented by two sticks connected at the oxygen atom, with a spring in between the sticks. This spring constrains the bond angle to some preferred bond angle θ_0, while the value of its spring constant k_2 (the *stiffness*) dictates how flexible the bond angle is. From the bond angle probability distribution $\mathcal{P}(\theta)$, it is possible to estimate the values of the preferred bond angle θ_0 and the bond angle stiffness k_2.

To extract the Si–O–Si bond angles from the data, we consider each O ion together with its two nearest Si neighbors and calculate the angle between the two Si–O bonds. In Fig. 6, we show the resulting probability distributions $\mathcal{P}(\theta)$ of the Si–O–Si angle θ for BKS and WAC at zero pressure. These curves have been measured before in previous studies[2,6] but with less detail. As the temperature decreases, the width of the distribution decreases and the maximum shifts toward 180°. This implies that the liquid becomes more structured and stiffer. This is to be expected, since at a high

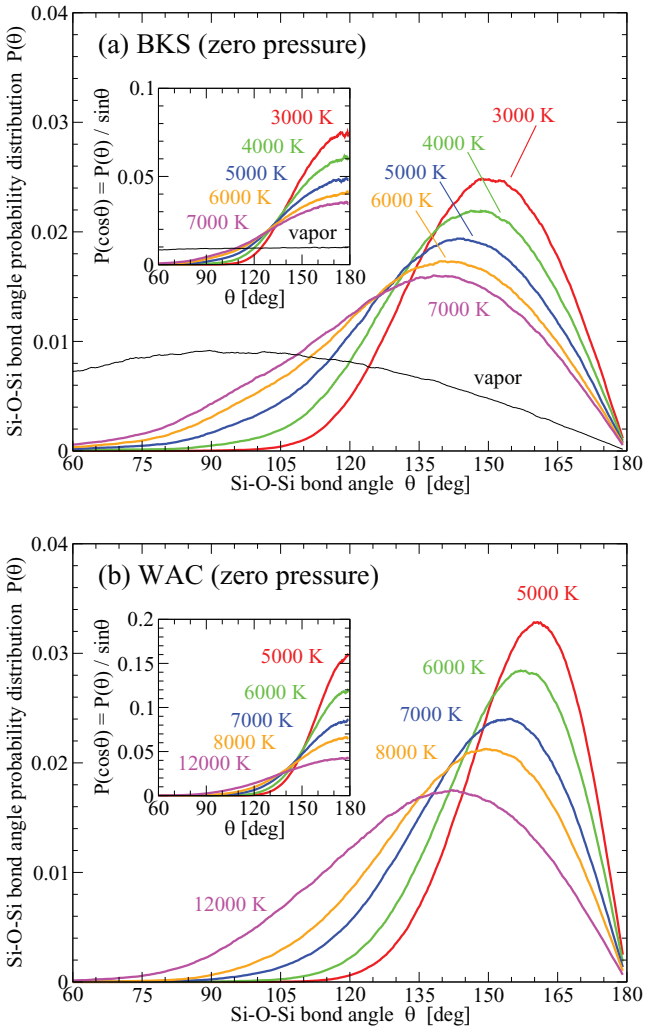

FIG. 6. Probability distribution of the Si–O–Si bond angle $\mathcal{P}(\theta)$ in liquid silica for (a) the BKS model and (b) the WAC model. As T goes down, the most probable angle moves closer to 180° while simultaneously the width of the distribution decreases. The first phenomenon causes the liquid to expand upon cooling, while a reduction in width means that the bonds become stiffer, which leads to a decrease in diffusion. Both phenomena are related (see below) and are much stronger for WAC than for BKS. Instead of $\mathcal{P}(\theta)$ it is better to consider $\mathcal{P}(\cos\theta) = \mathcal{P}(\theta)/\sin\theta$, since a completely random distribution such as in the vapor has $\mathcal{P}(\theta) \propto \sin\theta$, while $\mathcal{P}(\cos\theta)$ is uniform (see inset of panel (a)). For both models and all temperatures $\mathcal{P}(\cos\theta)$ resembles a normal distribution with mean 180°. This indicates that the preferred angle is in fact 180°, and that the width of $\mathcal{P}(\cos\theta)$ determines both the location of the peak in $\mathcal{P}(\theta)$ as well as its width.

temperatures there are more thermal fluctuations and therefore $\mathcal{P}(\theta)$ has a broader distribution.

Plotting $\mathcal{P}(\theta)$ may not be the best way of presenting the bond angle distribution, as this distribution is biased toward 90° angles. This is particularly clear from the distribution of the vapor (the thin black line in Fig. 6(a)). The ions in the vapor have no preferred position with respect to their neighbors, yet $\mathcal{P}(\theta)$ is not uniform but proportional to $\sin\theta$. This is related to the fact that the infinitesimal area element of the unit sphere is $dA = \sin\theta\, d\theta\, d\phi$ rather than $d\theta\, d\phi$. As $\theta \to 180°$ the area element dA approaches zero, and therefore $\mathcal{P}(\theta) = 0$ at $\theta = 180°$. Instead of $\mathcal{P}(\theta)$ it is better to consider the probability distribution $\mathcal{P}(\cos\theta) = \mathcal{P}(\theta)/\sin\theta$, as is shown in the insets of Fig. 6. The $\mathcal{P}(\cos\theta)$ distribution of the vapor is a uniform distribution (inset of Fig. 6(a)). For the liquid, the distribution $\mathcal{P}(\cos\theta)$ is approximately a normal distribution with its mean at $\theta_0 = 180°$. Evidently, the most probable inter-tetrahedral angle (the location of the $\mathcal{P}(\theta)$-peak) is purely an effect of the width of this normal distribution combined with the fact that $dA \propto \sin\theta$.

It is possible to interpret the bond angle distribution in terms of an effective potential $U_{\text{eff}}(\theta)$, assuming that $\mathcal{P}(\cos\theta) \propto \exp[-U_{\text{eff}}(\theta)/k_BT]$. When the effective potential is harmonic, i.e., $U_{\text{eff}} = \frac{1}{2}k_2(\theta - \theta_0)^2$, the resulting probability distribution is a normal distribution with mean θ_0 and a width that depends on temperature T and stiffness k_2. In general, the effective potential will not be perfectly harmonic and includes anharmonic terms. Because $\cos\theta$ is an even function about $\theta = 180°$, it is required that $\mathcal{P}(\cos\theta)$ is as well, and therefore also $U_{\text{eff}}(\theta)$. Consequently, the leading-order anharmonic term in $U_{\text{eff}}(\theta)$ is of the fourth order. The Si–O–Si bond angle distribution can thus be described by

$$\mathcal{P}(\theta) = A \sin\theta \exp[-U_{\text{eff}}(\theta)/k_BT] \tag{1}$$

with U_{eff} a Taylor series about the mean angle $\theta_0 = 180°$,

$$U_{\text{eff}}(\theta) = \frac{1}{2}k_2(\theta - \theta_0)^2 + \frac{1}{4!}k_4(\theta - \theta_0)^4 + \ldots. \tag{2}$$

Here A is a temperature-dependent normalization constant that ensures that the total probability $\int \mathcal{P}(\theta)\, d\theta = \int \mathcal{P}(\cos\theta)\, d\cos\theta$ is equal to one, and k_B is the Boltzmann constant.

The probability distributions of Fig. 6 can be fitted quite well with Eqs. (1) and (2), even when the sixth power and higher-order terms are ignored. The resulting values for the stiffness k_2 are shown in Fig. 7. It is immediately clear that WAC is far more rigid than BKS. For BKS the stiffness does not vary much with temperature, while increasing the pressure makes the bonds slightly less stiff. The same is true for WAC at high T, but below 5 GPa the stiffness shows an increase when the liquid is cooled. This increase is exactly where C_P has its maximum in Fig. 2(b), and thus we may argue that the increase in C_P is due to a structural change, namely, the stiffening of the tetrahedral network.

From the isochores in Fig. 1(b), it is clear that WAC is very close to having a LLCP. If we compare the results of previous studies done on tetrahedral liquids[30,34] with our results for BKS and WAC, then we see that the tetrahedrality of BKS is far too small (i.e., the inter-tetrahedral bond angles are not sufficiently stiff) to have a LLCP, and that WAC is close, but not close enough. However, it might be possible to make a small change to the WAC potential to enhance its tetrahedrality. One simple way to achieve this would be to add a repulsive term similar to the three-body interaction of the Stillinger-Weber model. This term should penalize any Si–O–Si configuration with an angle less than 180° with a repulsive energy determined by the intensity parameter λ and the size of the deviation. The λ value associated with this interaction should be carefully chosen; if λ is too small no LLCP will arise, while applying a λ that is too large will likely lead to crystallization into a diamond (β-cristobalite) structure. It would be interesting to see at what value of k_2 this

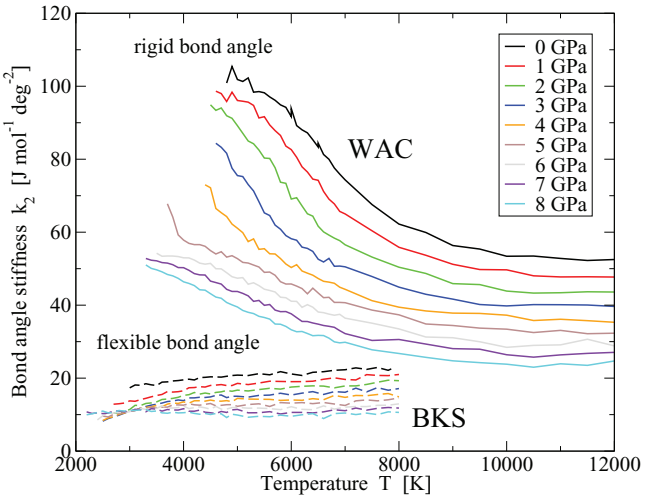

FIG. 7. Stiffness of the Si–O–Si bond angle for both WAC (solid lines, top) and BKS (dashed lines, bottom). For both models the stiffness k_2 goes down with increasing pressure. It is clear that BKS has more flexible bonds (small k_2), and that WAC is more rigid (large k_2) and therefore "more tetrahedral." In addition, WAC shows a transition at low T for $P \leq 5$ GPa to a state with an even higher stiffness.

criticality is introduced, and if this value is the same across other tetrahedral models as well, but this is beyond the scope of the present project.

The results presented here are also relevant to the possible existence of a LLCP in different water models, and highlight the importance of a thorough analysis of the O–H–O bond angle distribution. Such an analysis, possibly with the use of a bond angle stiffness parameter such as k_2, might be able to predict if a particular water model will have a LLCP. Unfortunately, to the best of our knowledge, it is currently not possible to measure these angles directly in experiments, as significant help from computer simulations is required to obtain the angular structure of liquid water.[41,42]

VI. CONCLUSION

Although it has been suggested, based on a combination of simulation and theoretical considerations,[18] that both BKS and WAC have LLCPs at temperatures beyond the accessible simulation range, our study suggests that neither BKS nor WAC can reach a critical point. We have compared our results to those of other tetrahedral models,[30,34] analyzed the bond angle distributions, and conclude that the lack of a LLCP in both BKS and WAC is due to a lack of stiffness in the inter-tetrahedral Si–O–Si bond angles. WAC is close to criticality, but BKS shows little sign of a LLCP, and since the latter is considered to be the more realistic model for experimental silica, we expect that no LLCP occurs in real silica either.

However, this does not mean that manifestations of criticality can never be observed. As Chatterjee and Debenedetti[43] have shown theoretically, even a weak tendency toward criticality (as in BKS) can be amplified into a liquid-liquid phase separation in a binary system. Indeed this notion has been exploited in Ref. 44 to interpret the (much-studied[45–51] but incompletely understood) splitting out of an almost pure SiO_2 phase from such simple systems as the Na_2O-SiO_2 and Li_2O-SiO_2 binary glasses during supercooling.

ACKNOWLEDGMENTS

We would like to thank P. Debenedetti, V. Molinero, H. Aragão, and C. Calero for the many valuable discussions. E.L. and H.E.S. thank the National Science Foundation (NSF) Chemistry Division for support (Grant No. CHE 12-13217) S.V.B. thanks the Dr. Bernard W. Gamson Computational Science Center at Yeshiva College for support. C.A.A. acknowledges the support of this research through the National Science Foundation (NSF) chemistry program under collaborative Grant No. CHE 12-13265.

APPENDIX A: WAC AND BKS SILICA

One of the simplest models for silica is the WAC model introduced by L. V. Woodcock, C. A. Angell, and P. Cheeseman.[21] The model is sometimes also known as the Transferable Ion Model (TRIM) because its potential is rather general and can also be used to model other ionic liquids.[52] In the WAC model, the material consists of a 1:2 mixture of Si^{+4} and O^{-2} ions, without any explicit bonds. Apart from the electrostatic force, the ions also interact with each other via an exponential term,

$$U_{\mathrm{WAC}}(r_{ij}) \equiv \frac{1}{4\pi\varepsilon_0}\frac{z_i z_j e^2}{r_{ij}} + a_{ij}\left(1+\frac{z_i}{n_i}+\frac{z_j}{n_j}\right) \times \exp\left[B_{ij}(\sigma_i+\sigma_j-r_{ij})\right]. \quad \text{(A1)}$$

Here the subscripts $i, j \in$ Si,O indicate the species of the two ions involved, z_i the charge of each ion ($z_{\mathrm{Si}} = +4$, $z_{\mathrm{O}} = -2$), $n_{\mathrm{Si}} = n_{\mathrm{O}} = 8$ the number of outer shell electrons, and σ_i the size of each ion ($\sigma_{\mathrm{Si}} = 0.1310$ nm, $\sigma_{\mathrm{O}} = 0.1420$ nm). For WAC silica the parameters a_{ij} and B_{ij} are the same for all pairs: $a_{ij} = 0.19$ perg $\approx$11.44 kJ/mol and $B_{ij} = 34.48$ nm^{-1}.[52] The potential can also be written as

$$U_{\mathrm{WAC}}(r_{ij}) = \frac{1}{4\pi\varepsilon_0}\frac{q_i q_j}{r_{ij}} + A_{ij}\exp(-B_{ij}r_{ij}), \quad \text{(A2)}$$

with $A_{\mathrm{SiSi}} = 1.917\,991\,469 \times 10^5$ kJ/mol, $A_{\mathrm{SiO}} = 1.751\,644\,217 \times 10^5$ kJ/mol, and $A_{\mathrm{OO}} = 1.023\,823\,519 \times 10^5$ kJ/mol.

The second model that we consider here is BKS, which is currently one of the most popular models for silica. The BKS model was introduced by B. W. H. van Beest, G. J. Kramer, and R. A. van Santen[1] and is similar to WAC. Silica is again modeled as a simple 1:2 mixture of Si- and O-ions, without explicit bonds. To produce results that better match experiments and *ab initio* simulations, and to be able to effectively represent screening effects, the charges in BKS are not integer values of e but instead are given by $q_{\mathrm{Si}} = +2.4e$ and $q_{\mathrm{O}} = -1.2e$. In addition to this, the BKS potential also differs from the WAC model in that it includes an attractive r^{-6} term

$$U_{\mathrm{BKS}}(r_{ij}) \equiv \frac{1}{4\pi\varepsilon_0}\frac{q_i q_j}{r_{ij}} + A_{ij}\exp(-B_{ij}r_{ij}) - C_{ij}r_{ij}^{-6}. \quad \text{(A3)}$$

TABLE I. Parameters of the modified BKS potential of Eq. (A4). Because Si–Si only has the (repulsive) Coulomb interaction, all parameters are zero for Si–Si. One mol here indicates one mol of ions, not one mol of SiO_2 molecules.

	Si–O	O–O	Units
a_{ij}	$2.678\,430\,850 \times 10^5$	$9.208\,901\,230 \times 10^4$	kJ/mol nm^2
b_{ij}	$-7.343\,377\,221 \times 10^4$	$-4.873\,373\,066 \times 10^4$	kJ/mol nm
c_{ij}	$2.353\,960\,789 \times 10^3$	$7.337\,042\,047 \times 10^3$	kJ/mol
A_{ij}	$1.737\,098\,076 \times 10^6$	$1.339\,961\,920 \times 10^5$	kJ/mol
B_{ij}	48.7318	27.6	nm^{-1}
C_{ij}	$1.288\,446\,484 \times 10^{-2}$	$1.688\,492\,907 \times 10^{-2}$	nm^6 kJ/mol
$U_{c,ij}$	$-0.465\,464\,470$	$-0.575\,753\,031$	kJ/mol
r_s	0.139 018 528	0.195 499 453	nm
r_c	0.55	0.55	nm

In BKS, there is no interaction between two Si-ions apart from the electrostatics, i.e., $A_{SiSi} = B_{SiSi} = C_{SiSi} = 0$. The A_{ij}, B_{ij}, and C_{ij} parameters for the Si-O and O-O interactions are listed in Table I and are exactly the same as in the original BKS model.

Although the BKS model has been quite successful in simulations of quartz and amorphous silica, at temperatures above ∼5000K two ions can come very close, causing problems. As $r \to \infty$ the BKS potential diverges to $-\infty$ and the two ions fuse together—a non-physical phenomenon that is an artifact of the model. One way to solve this issue is by including an additional repulsive term at very small r, e.g., by adding a r^{-30} term.[18] When such a large power is used, however, a small time step is required to prevent large forces, which leads to much slower simulations. Because of this, we instead adjust the BKS potential at small r by adding a second-degree polynomial for $r \le r_s$. Here r_s is the point at which the original BKS force has an inflection, i.e., where $d^2F_{BKS}/dr^2 = -d^3U_{BKS}/dr^3 = 0$. We choose the coefficients of the polynomial such that the new potential $U(r)$ has no inflection at $r = r_s$. Adding the polynomial still leads to $U(r) \to -\infty$ when $r \to 0$, but increases the height of the energy barrier sufficiently to allow us to simulate the high temperatures we wish to explore. Choosing a short-range correction to BKS has been found to have little effect on the simulation results, and merely prevents the ions from fusing.

To further speed up the simulations, we modify the BKS potential as described by K. Vollmayr, W. Kob, and K. Binder in Ref. 2, and truncate and shift the potential at $r_c = 0.55$ nm. Although this truncation leads to a shift in pressure, it otherwise produces approximately the same results.[2] In conclusion, the modified BKS potential we use is given by

$$U'_{BKS}(r_{ij}) = \frac{1}{4\pi\varepsilon_0}\frac{q_i q_j}{r_{ij}} + \begin{cases} a_{ij}r_{ij}^2 + b_{ij}r_{ij} + c_{ij} - \frac{1}{4\pi\varepsilon_0}\frac{q_i q_j}{r_{ij}} & (r_{ij} < r_s) \\ A_{ij}\exp(-B_{ij}r_{ij}) - C_{ij}r_{ij}^{-6} - U_{c,ij} & (r_s < r_{ij} < r_c) \\ 0 & (r_{ij} > r_c), \end{cases} \tag{A4}$$

with the parameter values for $ij = SiO$ and $ij = OO$ listed in Table I. For the Si–Si interaction the potential is $U'_{BKS}(r_{SiSi}) = \frac{1}{4\pi\varepsilon_0}q_{Si}^2/r_{ij}$ and does not involve any cutoffs, apart from the real-space cutoff of the Ewald sum.

APPENDIX B: CALCULATION OF RESPONSE FUNCTIONS VIA SURFACE FITS

In order to construct isobaric response functions from a large set of constant-volume (NVT) data, some type of fit or interpolation is needed. For example, to calculate $C_P = (\partial H/\partial T)_P$ we consider the enthalpy H as a function of both P and T and fit the data $[P, T, H]$ with a smooth three-dimensional surface $H(P, T)$. Abrupt changes in $H(P, T)$ lead to large spikes in its derivative $\partial H/\partial T$, and thus the $H(P, T)$ surface must be smooth if we are to obtain a meaningful C_P. Fitting a surface rather than a curve has the additional advantage that more data are taken into account, resulting in better statistics. An alternative approach is to calculate C_P via fluctuations in H, but it has been shown[25] that first fitting $H(T)$ and then taking a derivative leads to cleaner results. It is of course easier to calculate C_P by doing constant-pressure (NPT) simulations instead, but then one would have the same problem with calculating C_V. We conclude that we can easily calculate all response functions if we apply a smooth surface fit $f(x, y)$ to a set of three-dimensional points $z_k(x_k, y_k)$.

Fitting a surface to a set of points means striking a balance between the "smoothness" of the fit and the fitting error induced. One measure of smoothness is the Laplacian $\nabla^2 f$, since a small Laplacian means little change in the slope of $f(x, y)$, and thus a smoother function. Hence, to obtain a smooth surface fit $f(x, y)$ through the data points $z_k(x_k, y_k)$ with $k = 1, 2, \ldots, N$, we minimize

$$J = \sum_{k=1}^{N} w_k \left[f(x_k, y_k) - z_k \right]^2 + \iint \left| \nabla^2 f(x, y) \right|^2 dx\, dy. \tag{B1}$$

The weights w_k provide the balance between the smoothness and the fitting error. If we set w_k too low, we obtain a very smooth fitting function $f(x, y)$ that poorly represents the data. If we set w_k too high, the function $f(x, y)$ will go through all the data points but will show large variations. Because large variations in the surface lead to even larger variations in the derivatives, the $H(P, T)$ surface must be very smooth when we calculate the C_P. Fortunately, introducing small fitting errors does not cause problems, because the simulation data already suffer from small statistical errors. If the underlying response function is in fact smooth, then it is possible to use the fitting errors to partially cancel the statistical errors.

Minimization of the functional J in Eq. (B1) is not a new concept. For example, the CSAPS function in MATLAB applies a similar minimization scheme to calculate a cubic smoothing spline. As opposed to this MATLAB function, we do not impose the constraint that $f(x, y)$ is a tensor product spline, but instead represent $f(x, y)$ by a set of 100 × 100 points (x_i, y_j, f_{ij}) placed on a regular grid (x_i, y_j). Bilinear interpolation is used to estimate the value of $f(x, y)$ between these grid points, and the derivatives and the Laplacian are calculated using finite (central) differences. To compensate for the reduced number of data points near the edges of the

domain, we recommend that higher-order differences near the edges be used.

[1] B. W. H. van Beest, G. J. Kramer, and R. A. van Santen, Phys. Rev. Lett. **64**, 1955 (1990).
[2] K. Vollmayr, W. Kob, and K. Binder, Phys. Rev. B **54**, 15808 (1996).
[3] J. Horbach and W. Kob, Phys. Rev. B **60**, 3169 (1999).
[4] W. Götze, "Aspects of structural glass transitions," in *Liquids, Freezing and Glass Transition,* volume Session LI (1989) of *Les Houches Summer Schools of Theoretical Physics*, edited by J.-P. Hansen, D. Levesque, and J. Zinn-Justin (North-Holland, Amsterdam, 1991), pp. 287–503.
[5] W. Götze and L. Sjögren, Rep. Prog. Phys. **55**, 241 (1992).
[6] M. Hemmatti and C. A. Angell, "Comparison of pair potential models for the simulation of liquid SiO2: Thermodynamic, angular-distribution, and diffusional properties," in *Physics Meets Mineralogy: Condensed Matter Physics in the Geosciences*, edited by H. Aoki, Y. Syono, and R. J. Hemley (Cambridge University Press, Cambridge, England, 2000), Chap. 6.1, pp. 325–339.
[7] K.-U. Hess, D. B. Dingwell, and E. Rössler, Chem. Geol. **128**, 155 (1996).
[8] E. Rössler, K.-U. Hess, and V. N. Novikov, J. Non-Cryst. Solids **223**, 207 (1998).
[9] C. A. Angell, R. D. Bressel, M. Hemmatti, E. J. Sare, and J. C. Tucker, Phys. Chem. Chem. Phys. **2**, 1559 (2000).
[10] S. Sastry and C. A. Angell, Nat. Mater. **2**, 739 (2003).
[11] S. S. Ashwin, U. V. Waghmare, and S. Sastry, Phys. Rev. Lett. **92**, 175701 (2004).
[12] K. Ito, C. T. Moynihan, and C. A. Angell, Nature (London) **398**, 492 (1999).
[13] P. Gallo and M. Rovere, J. Chem. Phys. **137**, 164503 (2012).
[14] L. Xu, P. Kumar, S. V. Buldyrev, S.-H. Chen, P. H. Poole, F. Sciortino, and H. E. Stanley, Proc. Natl. Acad. Sci. U.S.A. **102**, 16558 (2005).
[15] C. Zhang, L. Hu, Y. Yue, and J. C. Mauro, J. Chem. Phys. **133**, 014508 (2010).
[16] K. N. Lad, N. Jakse, and A. Pasturel, J. Chem. Phys. **136**, 104509 (2012).
[17] P. H. Poole, M. Hemmati, and C. A. Angell, Phys. Rev. Lett. **79**, 2281 (1997).
[18] I. Saika-Voivod, F. Sciortino, and P. H. Poole, Phys. Rev. E **63**, 011202 (2000).
[19] C. A. Angell and M. Hemmati, "Glass transitions and critical points in orientationally disordered crystals and structural glassformers: ("Strong" liquids are more interesting than we thought)," AIP Conf. Proc. **1518**, 9 (2013).
[20] P. H. Poole, F. Sciortino, U. Essmann, and H. E. Stanley, Nature (London) **360**, 324 (1992).
[21] L. V. Woodcock, C. A. Angell, and P. Cheeseman, J. Chem. Phys. **65**, 1565 (1976).
[22] B. Hess, C. Kutzner, D. van der Spoel, and E. Lindahl, J. Chem. Theory Comput. **4**, 435 (2008).
[23] G. Bussi, D. Donadio, and M. Parrinello, J. Chem. Phys. **126**, 014101 (2007).
[24] T. A. Kesselring, E. Lascaris, G. Franzese, S. V. Buldyrev, H. J. Herrmann, and H. E. Stanley, J. Chem. Phys. **138**, 244506 (2013).
[25] E. Lascaris, T. A. Kesselring, G. Franzese, S. V. Buldyrev, H. J. Herrmann, and H. E. Stanley, "Response functions near the liquid-liquid critical point of ST2 water," AIP Conf. Proc. **1518**, 520–526 (2013).
[26] C. A. Angell, J. Non-Cryst. Solids **73**, 1 (1985).
[27] M. Hemmati, C. T. Moynihan, and C. A. Angell, J. Chem. Phys. **115**, 6663 (2001).
[28] P. Scheidler, W. Kob, A. Latz, J. Horbach, and K. Binder, Phys. Rev. B **63**, 104204 (2001).
[29] I. Saika-Voivod, P. H. Poole, and F. Sciortino, Nature (London) **412**, 514 (2001).
[30] V. Molinero, S. Sastry, and C. A. Angell, Phys. Rev. Lett. **97**, 075701 (2006).
[31] F. H. Stillinger and T. A. Weber, Phys. Rev. B **31**, 5262 (1985).
[32] V. V. Vasisht, S. Saw, and S. Sastry, Nat. Phys. **7**, 549 (2011).
[33] V. Kapko, private communication (2013).
[34] Y. Tu, S. V. Buldyrev, Z. Liu, H. Fang, and H. E. Stanley, Euro. Phys. Lett. **97**, 56005 (2012).
[35] N. Kern and D. Frenkel, J. Chem. Phys. **118**, 9882 (2003).
[36] F. Smallenburg and F. Sciortino, Nat. Phys. **9**, 554 (2013).
[37] V. Kapko, Z. Zhao, D. V. Matyushov, and C. A. Angell, J. Chem. Phys. **138**, 12A549 (2013).
[38] F. Romano, E. Sanz, and F. Sciortino, J. Chem. Phys. **134**, 174502 (2011).
[39] I. Saika-Voivod, F. Smallenburg, and F. Sciortino, J. Chem. Phys. **139**, 234901 (2013).
[40] J. R. Errington and P. G. Debenedetti, Nature (London) **409**, 318 (2001).
[41] K. A. Sharp and J. M. Vanderkooi, Acc. Chem. Res. **43**, 231 (2010).
[42] A. K. Soper and M. A. Ricci, Phys. Rev. Lett. **84**, 2881 (2000).
[43] S. Chatterjee and P. G. Debenedetti, J. Chem. Phys. **124**, 154503 (2006).
[44] C. A. Angell, P. H. Poole, and M. Hemmati, "A new interpretation of liquid-liquid unmixing in classical alkali silicate glasses," in *Proceedings of the 12th East European Glass Conference, Varna, Bulgaria*, edited by B. Samunova and Y. Demetriew (Publishing House "Science Invest," Sofia, 1997), pp. 100–109.
[45] R. J. Charles, J. Am. Ceram. Soc. **49**, 55 (1966).
[46] R. J. Charles, J. Am. Ceram. Soc. **50**, 631 (1967).
[47] R. J. Charles, Phys. Chem. Glasses **10**, 169 (1969).
[48] F. Y. Galakhov and B. G. Varshal, "Causes of phase separation in simple silicate systems," in *Phase-Separation Phenomena in Glasses*, The Structure of Glass Vol. 8, edited by E. A. Porai-Koshits (Consultants Bureau, New York, 1973), pp. 7–11.
[49] R. H. Doremus, *Glass Science* (Wiley, New York, 1973).
[50] W. Haller, D. H. Blackburn, and J. H. Simmons, J. Am. Ceram. Soc. **57**, 120 (1974).
[51] M. Morishita, A. Navrotsky, and M. C. Wilding, J. Am. Ceram. Soc. **87**, 1550 (2004).
[52] M. Hemmati and C. A. Angell, J. Non-Cryst. Solids **217**, 236 (1997).
[53] A. Skibinsky, S. V. Buldyrev, G. Franzese, G. Malescio, and H. E. Stanley, Phys. Rev. E **69**, 061206 (2004).
[54] P. H. Poole, I. Saika-Voivod, and F. Sciortino, J. Phys.: Condens. Matter **17**, L431 (2005).
[55] T. A. Kesselring, F. Franzese, S. V. Buldyrev, H. J. Herrmann, and H. E. Stanley, Nature Scientific Reports **2**, 474 (2012).
[56] L. Xu, S. V. Buldyrev, C. A. Angell, and H. E. Stanley, Phys. Rev. E **74**, 031108 (2006).